ENTE PER LE NUOVE TECNOLOGIE,
L'ENERGIA E L'AMBIENTE

ISSN / 1120 / 5571

Serie Innovazione

CHARACTERISATION OF SCINTILLATING GLASSY MATRICES FOR MIDDLE AND LOW ENERGY PHYSICS EXPERIMENTS

S. BACCARO, A. CEMMI

ENEA - Divisione Servizi Tecnologici
Centro Ricerche Casaccia, Roma

A. CECILIA

INFN - Sezione di Roma

RT/INN/2000/4

ENTE PER LE NUOVE TECNOLOGIE,
L'ENERGIA E L'AMBIENTE

Serie Innovazione

CHARACTERISATION OF SCINTILLATING GLASSY MATRICES FOR MIDDLE AND LOW ENERGY PHYSICS EXPERIMENTS

S. BACCARO, A. CEMMI

ENEA - Divisione Servizi Tecnologici
Centro Ricerche Casaccia, Roma

A. CECILIA

INFN - Sezione di Roma

RT/INN/2000/4

CARATTERIZZAZIONE DI MATRICI VETROSE SCINTILLANTI PER ESPERIMENTI DI FISICA DI MEDIA E BASSA ENERGIA

Riassunto

Gli scintillatori vetrosi rappresentano un'interessante alternativa ai cristalli scintillanti per il loro basso costo di produzione e facilità di lavorazione. Gli unici problemi connessi all'utilizzo di questo tipo di materiali sono:

- una bassa efficienza di trasferimento di energia, che è il motivo del basso valore di light yield delle matrici vetrose rispetto ai cristalli scintillanti;
- una bassa resistenza alla radiazione.

Gli attivatori che più comunemente vengono utilizzati nelle matrici vetrose sono il cerio ed il terbio trivalenti (con il gadolinio come costituente in alcune composizioni) che sono caratterizzati da una luminescenza nelle regioni spettrali UV-BLUE e VERDE-ROSSO rispettivamente. L'obiettivo di questo lavoro è studiare la dipendenza della resistenza alla radiazione di vetri fosfati e silicati dalle concentrazioni di drogante (Ce^{3+} or Tb^{3+}) e dalla composizione della matrice. I campioni sono stati anche sottoposti a misure di fotoluminescenza eseguite utilizzando un laser ad eccimeri (XeCl, 308 nm) per ottenere possibili evidenze del trasferimento di energia dal gadolinio al centro luminescente.

Parole chiave: Scintillatore, Luminescenza, Attivatore, Matrice vetrosa, Resistenza alla radiazione.

CHARACTERISATION OF SCINTILLATING GLASSY MATRICES FOR MIDDLEAND LOW ENERGY PHYSICS EXPERIMENTS

Abstract

Scintillators based on glassy matrix are of great interest due to their lower production cost with respect to single crystal systems and easy shaping of elements. In spite of the interest towards these materials, essential problems of glassy matrix exist and consist in the following:

- *low transfer efficiency, which is the reason for rather low Light Yield observed in glass scintillator with respect to single crystal system;*
- *low radiation hardness.*

Trivalent cerium and terbium are frequently used activators (with trivalent gadolinium as the constituent cation in some compositions) causing emission in UV-BLUE and GREEN-RED spectral region respectively. The aim of this work is to study the dependence of silicate and phosphate glasses radiation hardness on the dopant (Ce^{3+} or Tb^{3+}) concentrations and on the composition of the glass matrix. Furthermore photoluminescence decay measurements were performed with excimer laser (XeCl, 308 nm) to obtain possible evidences about energy transfer from Gd^{3+} ions to luminescent centres.

Keywords: Scintillator, Luminescence, Activator, Glassy matrix, Radiation hardness.

Index

Introduction

Detection of ionising radiation throughout the collection of light produced in scintillating materials, is a widely used technique in the field of radiation monitoring, medical imaging, geophysical and space explorations. Moreover, scintillators are used in Low and High Energy Physics experiments; they are generally carried out from very pure materials and are submitted to great study whether from the science of materials or from the application point of view. In some applications, scintillating crystals can be replaced by opportunely doped glassy matrices, with a sufficiently high density and good chemical and mechanical stability. Glassy scintillators can be used in detection of low and middle energy radiation (until 1 MeV). In particular, heavy ions doped glasses can be used for X-rays detection, while for neutron detection light ions doped matrices are necessary. The advantages connected to glasses utilisation are their low production cost and easy shaping of elements. Problems bound to the use of these materials are their low light production (Light Yield) due to a low efficiency in energy transfer (as we will explain later) and low radiation hardness.

This work concerns the study of luminescence and scintillation of glassy matrices used in X-ray detection until middle energy. In particular, Ce^{3+} and Tb^{3+} doped matrices were studied in order to find some correlation between doping and radiation damage. Measurements reported in this work were carried out in a collaboration that involves the Sezione INFN Roma, ENEA (INN/TEC/IRR), the Sezione INFN Padova, the Stazione Sperimentale del Vetro of Murano (Venice) and the Institute of Physics of Academic Science of Prague. This work was also the argument of an International University Master thesis in Nuclear and Ionising Radiation Technology (University of Pavia).

Chapter 1 - Scintillator detectors: basic principles

A scintillator is a material able to convert energy lost by ionising radiation into pulses of light. In several scintillation counting applications, ionising radiation is in the form of X-rays, γ-rays and α or β particles ranging from few thousands of eV to some billions of eV. Pulses of light emitted by scintillating material can be detected by a sensitive light detector, usually a photomultiplier tube (PMT), a photodiode (PD), or avalanche photodiode (APD). The combination of scintillator and light detector is called *scintillation detector*. The ideal scintillation material should have the following properties:

- it should convert the kinetic energy of charged particles into detectable light with a high scintillation efficiency;
- this conversion should be linear – the Light Yield should be proportional to deposited energy over a range as wide as possible;
- the medium should be transparent to the wavelength of its own emission for good light collection;
- the decay time of the induced luminescence should be short so that fast signal pulses can be generated;
- the material should have good optical quality and manufactured in size large enough to be of interest as a practical detector;
- its refractive index should be similar to the glass one (around 1.5) to allow efficient collecting of scintillation light.

Since no material will meet all these criteria simultaneously, the choice of a particular scintillator is always a compromise among these and other factors. Scintillator working is based on the fluorescence process, that consists in prompt emission of visible light from a substance following its excitation by some means. It is conventional to distinguish several other processes that can also lead to visible light emission:

- phosphorescence process corresponds to longer wavelength light emission than fluorescence, with a generally much slower characteristic time;
- delayed fluorescence results in the same emission spectrum as prompt fluorescence, but again is characterised by a much longer emission time.

To be a good scintillator, a material should convert a fraction as large as possible of the incident radiation energy to prompt fluorescence, minimising the generally undesirable phosphorescence and delayed fluorescence contribution.

In order to better understand these processes, next paragraph will concern the problem of luminescence processes related to structural properties of solids.

1.1 Luminescence processes in solids

Inorganic scintillators are generally carried out from single crystals (or glassy matrices), in which luminescence comes from emission centres already present in the structure or from activator agents introduced in the crystal lattice in controlled way [1]. To clarify luminescence process, it is necessary retaking the crystal structure electronic bands model [2, 3].

1.1.1 Perfect crystals

The atomic or molecular electronic energy states consist in a series of discrete levels defined by Schröedinger's equation. In inorganic crystal lattice, the outer electronic energy levels are perturbed by mutual interactions between the constituent atoms or ions, and electrons are placed in a series of continuos "allowed" energy bands, separated by "forbidden" energy regions.

The atomic inner electronic levels are practically undisturbed and retain their normal character. A schematic diagram of ionic crystal insulator energy band model is shown in Fig. 1.1. In the normal state the lower energy bands are completely filled and the higher bands do not contribute to electrical conduction, since equal number of electrons moves in opposite directions [4].

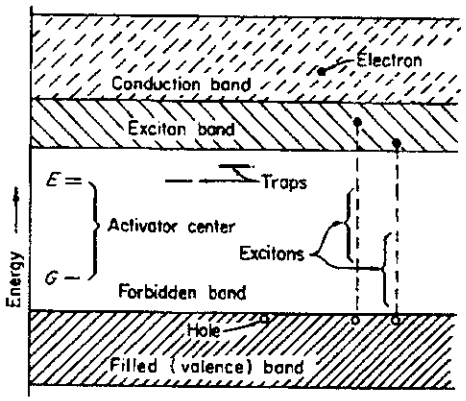

Fig. 1.1: Conduction, valence and exciton bands in a crystal lattice [4].

The highest filled band, named valence band, is separated from the lowest empty band, named conduction band, by a few eV energy gap (E_g). Valence band electrons may be raised into conduction band by absorption of quanta leaving positive holes in valence band. Consequently photoconduction may occur due to independent motion of electrons in conduction band and of holes in valence band. Alternatively, excited electron can remain bound to positive hole constituting an exciton, that carries no net charge but migrates freely through crystal lattice. Moreover exciton can be formed by recombination of one electron in conduction band and one hole in valence band, already present in crystal structure. In semiconductor the energy gap is low enough to allow the electrons migration in valence band by thermal excitation. Oppositely, in insulator the energy gap is so high that the electrons number present in conduction band is negligible.

1.1.2 Imperfect crystals

Model described in the previous chapter can be applied only to insulator having a perfect crystal lattice. In practice, energy bands variations due to lattice defects and impurities occur, producing local electronic energy levels in normally forbidden region between conduction and valence bands. If these levels are unoccupied, electrons (or excitons) moving in the conduction band may enter them. These induced centres are (Fig. 1.2):

- luminescence centres, in which the transition to the ground state is accompanied by photon emission;
- quenching centres, in which radiationless thermal dissipation of energy may occur;
- traps, that are metastable levels from which electrons (or excitons) may return to conduction band by thermal energy acquisition from lattice vibrations, or may fall in valence band by radiationless transition.

The same centre can contain luminescence, quenching and/or trapping levels, their relative population being determined by the Boltzman statistical distribution.

The luminescence and quenching centres arise from impurities, interstitial ions and/or defects, and they introduce local discrete energy levels corresponding to ground and excited states of centre. Centre excitation can be induced by electron or hole capture from conduction or

valence band respectively, either simultaneously capture of exciton, or by electron-hole recombination.

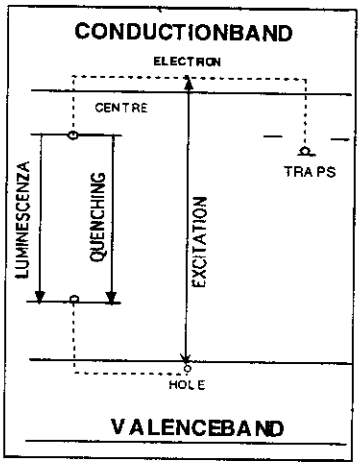

Fig. 1.2: Luminescence, quenching and trap centres in crystal forbidden gap.

Traps can be due to foreign ions (impurities), point lattice defects or dislocations present in crystal lattice. These defects create discrete energy levels in the forbidden band where electrons, holes or excitons can be entrapped, increasing their mean life. These traps may be subsequently emptied by optical or thermal excitation.
Frequently solid scintillators are doped with trivalent impurities (as Ce^{3+}, Tb^{3+}, Eu^{3+}...) that increase light emission probability during diseccitation process. These impurities, called "activators", create particular crystal lattice sites that modify its band structure. The energy difference between activators levels is lower than crystal energy gap; hence, electrons pass easily from the activator excited state to the fundamental one giving rise to visible light emission, increasing the scintillator performances (Fig. 1.3).

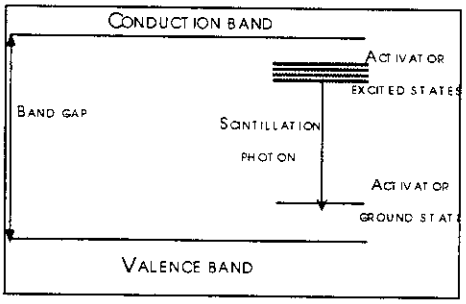

Fig. 1.3: Activator energy levels disposition in the forbidden band.

Every lattice periodicity deviation represents an imperfection and influences main solids properties (conductivity, coloration, plasticity). The most common defects are:
- volume defects, which differ in orientation (grains) from the rest of the lattice;
- structural defects (different phases);
- composition defects (precipitates);
- area defects, due to free surfaces, interfaces and accumulated defects;
- linear defects or dislocations;
- point defects (interstitial or substitutional ions, lattice vacancies, chemical impurities) [3].

This paper will concern principally point defects, because they are more interesting for scintillators, especially for ionising radiation application.

Frenkel and Schottky defects

In Fig. 1.4 we reported a two-dimensional crystal lattice representation in which two different interstitial ions (M^+,X^-) are present.

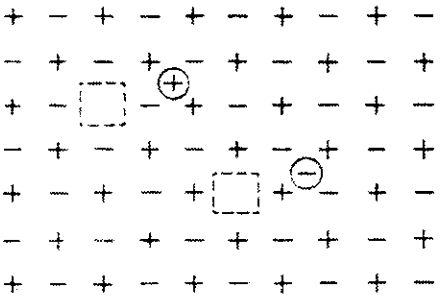

Fig. 1.4: Frenkel defects [4]

They arise when a cation or an anion are removed from their normal lattice sites by some processes and placed in an inter-lattice position normally free. This defect formation mechanism is called 'Frenkel mechanism' and the dual imperfection, the interstitial ion together with the vacancy, is known as "Frenkel defect". Vacant lattice sites in a crystal may be formed in another way, which does not involve interstitial ions production. This is illustrated in Fig. 1.5, where cations and anions are both removed from the interior of the crystal and added to the its surface to form a new layer. In order for this process to occur appreciably, equal number of cations and anions must be placed on the surface to preserve electrical neutrality, and hence equal concentration of cation and anion vacancies are produced in crystal interior. This mechanism of vacancy production was suggested by Wagner and Schottky and the dual imperfection consisting of a cation vacancy and an anion vacancy is known as "Schottky defect" [4]. In both cases, the electroneutrality of the crystal is preserved and there is a diminishing of the crystal density only for the Schottky defects.

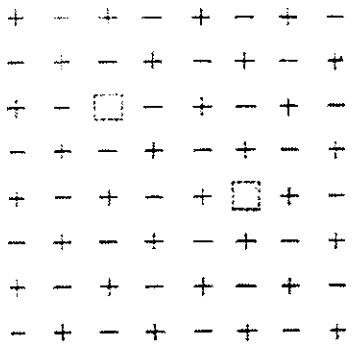

Fig. 1.5: Schottky defect [4].

Frenkel and Schottky defects arise in perfect crystals just for thermodynamic reasons because a crystal is at thermodynamic equilibrium if its free energy is minimum. In fact, although energy must be spent in order to form defects against the crystal cohesive forces, the increase in entropy coming from the defects causes the free energy be at minimum for a definite concentration of defects at a given temperature [4]. In general, cationic Frenkel defects are expected to form more easily than anionic ones, because the ionic radius of anions is greater than the cationic one and because of this the necessary energy to move anions in interstitial

positions is greater. The energy necessary to form respectively Frenkel and Schottky defects will be different, hence we will have a greater concentration of defects involving minimum energy activation.

Chemical impurities

Vacancies or interstitial ions can be produced also by introduction of foreign ions, namely chemical impurities. An example of these defects is shown in Fig. 1.6 for a two-dimensional polar crystal composed of monovalent ions, with some cations replaced at random by divalent positive ion impurities. The substitution of a monovalent cation with a divalent one places an extra positive charge in the crystal; hence, to preserve the electrical neutrality of the crystal as a whole, an extra negative ion must be incorporated interstitially or a positive ion vacancy must be formed at lattice point. The concentration of impurity defects is independent on temperature, being only determined by the concentration of foreign ions.

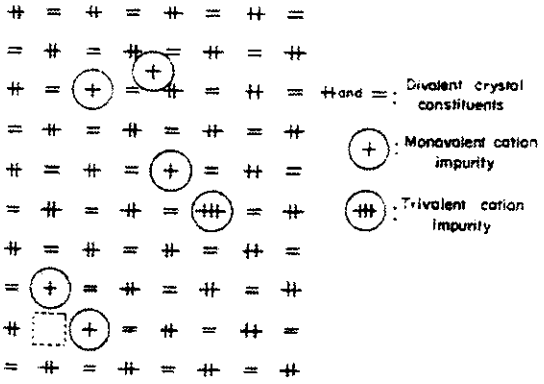

Fig. 1.6: Examples of chemical impurities in a crystal [4].

Vacancies couples and complex defects

From the previous section, one can deduce that vacancies and interstitial ions are regions in which a charge unsettling is localised: a cationic vacancy takes an effective negative and an anionic vacancy an effective positive charge. This situation implies an electrostatic attraction between two defects situated on adjacent sites, inducing possible double vacancy or couple formation [1]. These couples have no effective charge and do not contribute to electrical conductivity while, moving freely in the crystal lattice, occur in diffusion processes. In a similar way, one can attend a crystal impurity to associate with an adjacent defect producing complex defects (Fig. 1.7).

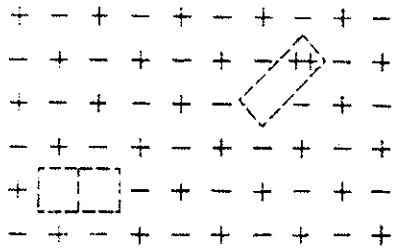

Fig. 1.7: Couples of vacancies and complex defects [4]

Colour centres

Solid pure matrices are generally transparent in the whole visible region. Solids can be coloured in different ways: by introducing chemical impurities or metallic ions excess, by electrolysis processes, or by irradiation with X-rays, γ-rays, neutrons and electrons.

During irradiation some electrons will be pulled away from crystal ions and it will induce the formation of an equal number of electrons and positive holes. Some electrons will rapidly recombine with holes and form again the primary ions. If, before this recombination, a free electron passes near an interstitial cation (or anionic vacancy, or cationic impurity with a valence greater than the lattice cation) this positive charged defect can entrap the electron in its Coulomb field. The same process involves also positive holes, entrapped from negative charged defect, as cationic vacancy and interstitial anions. Centres formed by entrapped electrons or holes can be bleached by heating (thermal-bleaching) or by irradiation with an appropriate wavelength light (photo-bleaching). The main effect of radiation-matter interaction is colour centres formation; these defects are able to absorb visible light [5].
Centres F: the simplest colour centres is called 'F centre' and is composed by an anion vacancy connected to an electron in excess present into the crystal Fig. 1.8. This electron will be delocalized on the positive ions surrounding the lattice vacancy.

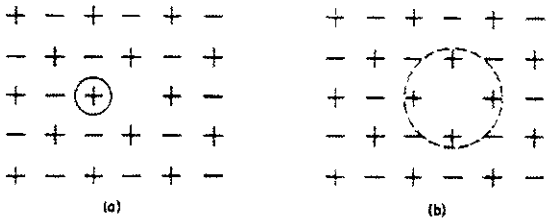

Fig. 1.8: Possible representation of an F centre:
(a) anionic vacancy connected to an electron in excess;
(b) negative charge delocalised on adjacent sites [4].

The association of two F centres constitutes an M centre, while three adjacent F centres an R centre. These centres can be generally distinguished by their optical properties.
Centre V_k: a 'V_k centre' is formed when a hole is entrapped from a couple of negative ions. The stable condition, identified by ESR measurements, is similar to a negative alogen ion molecule, that is Cl_2^- in KCl. In the V_k centre formation do not occur lattice vacancies or other ions. In a crystal other colour centres can be present (like 'V_1 centre' or 'H centre') analogous to a V_k centre, although less common.

1.1.3 Glassy matrices structure

A crystal structure can be represented as an infinite repetition, in the three space dimensions, of an elementary cell (or fundamental unit) that contains all symmetry elements present in the lattice. The regularity of this structure can be studied with X-ray diffraction and, at macroscopic level, by the geometric shape of the crystal. On the contrary, glassy matrices do not show a similar regular and definite structure; the first model for the representation of an inorganic glass was proposed by Zachariasen and Warren [4]. In this model, structural unities of a glassy compound are identical to the unities of the equivalent lattice, but the glassy structure is characterised by a long range order in the three dimensions. Moreover in the glassy matrix, interstices can be easily formed, which give hospitality to foreign ions of different valence or entrap one or more charge carriers. Obviously all these variations induce enlargement of absorption bands (due to impurity ions or colour centres) respect to the crystal structure [6]. This enlargement, more pronounced respect to the thermal one, is caused by different local electronic situations in which the responsible species can be situated.

1.2 Physical principles of scintillation mechanism

The scintillation mechanism is considered as a three steps process [7]:

1. Absorption of ionising radiation and energy conversion into electron-hole pairs.
2. Absorbed energy conversion to luminescence centres (which will pass to an emitting state).
3. Emission process (luminescence centres return from emitting state to ground state).

Absorption

The intensity of a monoenergetic gamma ray beam entering a detector of thickness d, is reduced in intensity according to the Beer-Lambert law:

$$I(E) = I_0(E) \cdot e^{-\mu(E)x} \tag{1.1}$$

where $I_0(E)$ is the impinging light intensity, I(E) the light intensity at a distance d and •(E) is the mass attenuation coefficient given by:

$$\mu(E) = \frac{N}{A} \cdot \sigma_{tot} \tag{1.2}$$

where N =Avogadro number, A =atomic weight of the material and σ_{tot} is the total cross section, or the sum of all the interaction cross-sections associated with physical processes that can occur during interaction: photoelectric effect, Compton scattering and pair production. The relative probability for the three processes is energy dependent: photoelectric effect is dominant between 0.01 and 0.5 MeV, Compton scattering is the main process between 0.5 and 4 MeV and pair production is the more probable interaction process between 5 MeV and 10 MeV [8]. Moreover these processes are accompanied by secondary processes such as the Auger emission and fluorescence (in photoelectric effect), recoil electrons emission (in Compton scattering) and positron annihilation (in pair production).

Photoelectric effect

Photoelectric effect consists in quantum energy absorption by an atom, with a subsequent electron emission from an electronic shell. The ejected electron (photo-electron) acquires an energy E_{pe} equal to the difference between the hν photon energy and the E_b electron binding energy ($E_{pe} = h\nu - E_b$). The photoelectric effect is more probable for deeply atomic electrons as K electrons, that constitute the greater part of the emitted electrons. The cross section for this process is monotonically decreasing with energy, with sudden spikes in correspondence of edges energy shells (K, L, M...). These energies are given by the Moseley law:

$$E_n = Rhc \frac{(Z-\sigma)^2}{n^2} \tag{1.3}$$

with Rhc =13.605 eV, Z = atomic number, σ = screen constant and n = principal quantum number [9]. A precise photoelectric cross section evaluation is not possible for all photon energies, but different empirical laws are suitable to describe this effect at various energies [10].

Compton effect

In the Compton effect, the photon interacts with an atomic electron and part of its energy is transferred to this electron. The result is a Compton scattered photon with energy $E_.=h\nu'$ and a so called 'Compton electron' with energy E_c (Fig. 1.9).

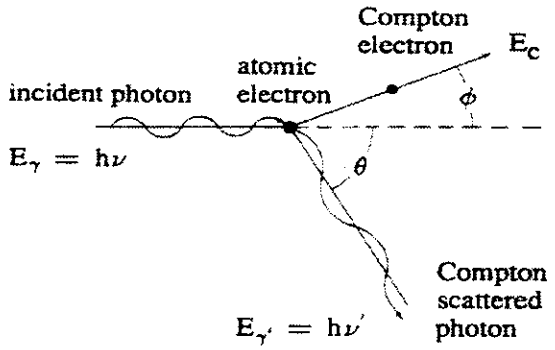

Fig. 1.9: Compton effect [12].

The energy distribution depends on the angle θ between the original photon direction and the scattered one. From conservation of momentum and energy, following equation can be derived:

$$E_{\gamma'} = \frac{E_\gamma}{1+\alpha(1-\cos\theta)} \tag{1.4}$$

where $\alpha = E_\gamma/0.511$ and E_γ and $E_{\gamma'}$ are expressed in MeV. The Compton electron energy is given by:

$$E_c = E_\gamma - E_{\gamma'} = \frac{\alpha(1-\cos\theta)}{1+\alpha(1-\cos\theta)} E_\gamma \tag{1.5}$$

From these relations we can deduce that the Compton electron energy attains the greatest value at θ=0 given by:

$$E_{c(\max)} = \frac{E_\gamma}{1+\dfrac{0.511}{2E_\gamma}} MeV \tag{1.6}$$

Pair Production

The pair production process may take place in electron or nucleus field [9, 11]: in the first case the electron energy should be greater than $4m_0c^2$, in the second greater than $2m_0c^2$. From this interaction process, a positron-electron pair is created and the positron annihilates with an electron producing two 0.511 MeV energy photons. The pair production cross section is given by:

$$\tau = 4Z^2\alpha r_e^2 f(E,Z) \tag{1.7}$$

where f(E,Z) is a slowly variable function depending on screen electrons, α is the fine structure constant, Z is the atomic number and r_c is the classical electron radius [12]. Hence, we can derive the mean free path of photon interaction:

$$\lambda_{pair} = \frac{1}{N\tau} \tag{1.8}$$

where N is the atomic density and τ is the pair production cross section; it is connected to radiation length by this relation:

$$\lambda_{pair} = \frac{9}{7} L_{rad} \tag{1.9}$$

where the radiation length is the path after which an electron, loosing energy by radiation, reduces its initial energy of a factor e.

Total cross section: the probability of X or γ photon interaction with matter is given by the sum of all cross sections related to photoelectric effect, Compton scattering and pair production:

$$\sigma_{tot} = \phi_{photo} + Z\sigma_c + \tau_{pair} \tag{1.10}$$

where Compton cross section is multiplied by Z, in order to take into account of all atomic electrons [13]. The total attenuation coefficient, μ, is given by:

$$\mu = N\sigma_{tot} \tag{1.11}$$

where N is the atomic density.

If a photon beam I_0 impinges on a material of thickness x, the transmitted beam is given by:

$$I = I_0 e^{-N\sigma x} = I_0 e^{-\mu x} \tag{1.12}$$

In general there is no rule that defines the absorption coefficient versus atomic number; approximately, we can assume that if the photoelectric effect is dominant:

$$\mu \propto Z^5 \tag{1.13}$$

At intermediate energies, where Compton scattering has the predominance:

$$\mu \propto Z \tag{1.14}$$

At higher energies, where pair production is dominant:

$$\mu \propto Z^2 \tag{1.15}$$

The probability cross section of these processes is reported in Fig. 1.11 versus absorber atomic number and energy; from this picture it is evident the dominance of Compton scattering between 0.8 and 4.0 MeV [11].

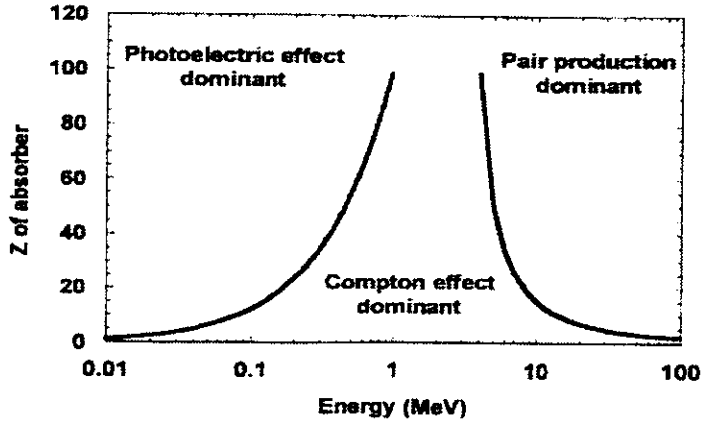

Fig. 1.11: Dominance of photoelectric, Compton and pair production processes versus energy and atomic number [11].

Conversion

When a high energy particle interacts with matter, it creates secondary electron-hole pairs by different processes. These produced charge carriers may transfer their energy to luminescent centres (most probably the process is lattice assisted) giving rise to light emission. The scintillation efficiency (η) is defined as the number of light photon emitted for 1 MeV of deposited energy and it is given by:

$$\eta = \beta S Q \tag{1.16}$$

where:

-β is the conversion efficiency of high energy photons into electron-hole pairs,

-S is the transport probability of thermalized electron-hole pairs (or excitons) towards emission centres, and
-Q is the radiative emission probability of emission centres themselves.
For a crystal with a band gap E_g, the mean necessary energy to create an electron-hole pair is:

$$E = \beta E_g \tag{1.17}$$

where β is always greater than 1 (β=3 for semiconductors). From this we can deduce that for deposited energy E_γ, the number of electron-hole pairs is given by:

$$n_{e-h} = \frac{E_\gamma}{\beta E_g} \tag{1.18}$$

and the photon number emitted by the crystal will be:

$$n_p = SQn_{e-h} \tag{1.19}$$

Hence, the scintillation effectiveness will be:

$$\eta = \frac{n_p}{E_\gamma} = \frac{SQ}{\beta E_g} \tag{1.20}$$

The transfer process complexity implies that S value cannot be predicted theoretically while Q value is close to 1 for many scintillators. The energy conversion process takes place in a very short time (ps) and the last step of the process itself (when electrons and holes have thermal energies between 10 and 100 eV) is the most important because it influences the scintillator performance.

Emission

This is the last scintillation process step and consists in emission centre returning to fundamental state from the excited one; if the de-excitation from this state occurs radiatively, we are dealing with a scintillation process.

Chapter 2-Characteristic parameters of scintillators

The most common parameters used for scintillator characterisation are Light Yield, emission spectrum and time decay. These parameters are defined in this way:

1. **Light Yield (LY):** it is the number of emitted photoelectrons (pe) per MeV of absorbed energy in a defined time interval (100 ns-10 μs) and can be expressed in pe/MeV. It depends on material scintillation efficiency, photomultiplier spectral sensibility and coupling efficiency between scintillator and photocatode.
2. **Emission spectrum:** it is characterised by two parameters:
   λ_m, the wavelength at the maximum emission;
   $\Delta\lambda$, the full width half maximum (FWHM).
3. **Time decay** (τ)**:** it represents the scintillator impulse amplitude and it is given by the process decay constant.

For a complete scintillator characterisation it is necessary to take into account some more parameters. Some of these are characteristic of the material itself (density, hygroscopicity, refraction index and hardness) but for radiation detection application field the most important properties are radiation length, Molière radius and radiation induced absorption coefficient, defined as follows:

Radiation length (X_0): it is the electron free mean path in a material, and depends on density, atomic mass and material atomic number. The mean free path length of an high energy photon is determined by the pair production process and is around $9X_0/7$.

Molière radius (R_m): it describes the lateral development of the electromagnetic shower, principally due to electrons and produced in a material from an high energy particle. Generally R_m can be approximated with the cylinder radius having axis coincident with shower symmetry axis and containing 95% of the total energy deposited in the material. In order to avoid superposition of adjacent electromagnetic showers (pile-up) it is required an R_m value as low as possible.

Radiation induced absorption coefficient (μ)**:**this parameter is connected to scintillator radiation hardness and represents the colour centres density induced in the structure by irradiation; it is given by:

$$\mu(\lambda) = \frac{1}{d}\ln\left[\frac{T_0(\lambda)}{T_{irr}(\lambda)}\right] \tag{2.1}$$

where T_0 and T_{irr} indicate transmission curves before and after irradiation and d the optical path in the sample (expressed in m). Some other factors can influence transmission decreasing: there can be reflection phenomenon due to index refraction differences in materials, interface problems (scattering, corner); intrinsic absorption of the material (absorption bands, scattering centres). Moreover, besides the intensity value of μ, it is important to study the variation of induced radiation damage in the time, or the $\mu(\lambda,t)$, and possibly to correlate it with LY.

Chapter 3- Techniques for scintillators analysis

Scintillator characterisation is carried out through steady state and time dependent parameters analysis. The steady state characterisation is performed by transmission, emission and excitation spectra measurements (generally acquired at room temperature). Time dependent properties are deduced from Light Yield, scintillation decay and photoluminescence decay measurements. In the last case, decay emission intensity can be approximated by a muliexponential interpolation:

$$I(t) = \Sigma A_i \exp\left(-\frac{t}{\tau_i}\right) \tag{3.1}$$

where τ_i is the decay time and A_i the signal intensity. Other techniques used to have a complete scintillator analysis are radioluminescence, thermostimulated luminescence (TSL) and thermostimulated current (TSC).
In this section we will discuss the used experimental techniques for scintillating glasses study.

Photoluminescence: this technique consists in material excitation by photon absorption, in order to obtain a scintillation emission spectrum for qualitative and quantitative analysis. The photoluminescence term refers to fluorescence and phosphorescence physical processes analysis, and is a really selective method that can be applied to many substances. One of the most used method is the luminescence time decay monocromatic analysis with single photon counting. At IROE-CNR Research Centre (Florence) we performed fluorescence measurements on glassy materials, in the temperature range between 18-300 K. An excimer laser source (XeCl, 308 nm) was used and the emission was observed at 90° by a PC driven spectrometer with two interchangeable gratings with different resolution and possibility of commuting on two channel (Fig. 3.1). In the first channel, a fast photomultiplier (2 ns) allows to collect the decay emission curve that is analysed by a digital sampling oscilloscope (Tektronix TDS 680D) giving time decays on a temporal scale ranging from ns to s. On the second channel an Optical Multichannel Analyzer (OMA) EG&G PARC 1461 allows to obtain emission spectra between 250-800 nm, in continuos way (CW) or in time resolved way (TR, with windows of 20 ns or greater).

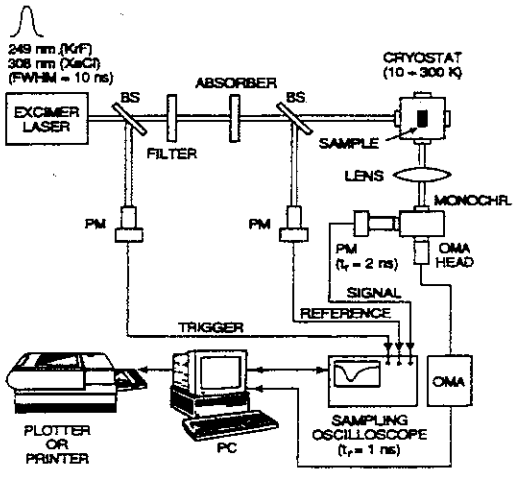

Fig. 3.1: Experimental set-up for luminescence measurements (IROE-CNR).

Optical transmission: this technique is useful to identify possible scintillator absorption bands that overlap with luminescence spectrum inducing an energy resolution decrease [14]. In particular, for our measurements, we used a double ray spectrophotometer [15] Perkin Elmer 340 UV-VIS-NIR, in wavelength range 190 ÷2600 nm, connected to a PC. In the ultraviolet range a deuterium lamp is used, while in visible and near-infrared region a tungsten one.

Light Yield measurements: Light Yield measurements were performed in the Laboratories of Physics Department (University "La Sapienza", Rome). The main component of Light Yield experimental set-up (Fig. 3.2) is a multichannel analyser that produces an histogram relative to photon energy absorption in the scintillator throughout photoelectric, Compton and pair production processes.

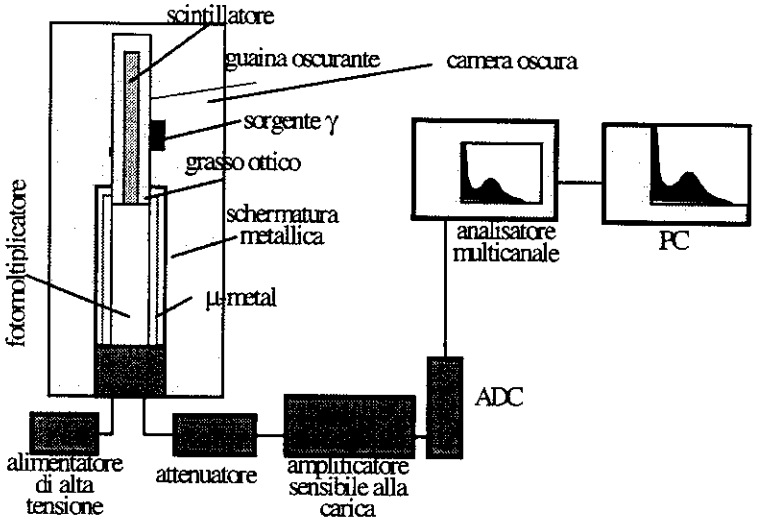

Fig. 3.2: Experimental set-up for Light Yield measurement.

An example of absorption spectrum is shown in Fig. 3.3 for a BGO crystal and a ^{137}Cs source. We can easily distinguish a peak (named photoelectric peak) due to total absorption of incident photon energy by photoelectric effect. For the Compton effect we can distinguish a kind of "shoulder", named Compton continuum, ranging from 0 to the maximum transferable energy value to an electron in a Compton collision (named Compton edge).
During pair production process, two 0.511 MeV photons are emitted. We can distinguish three cases:

1) if both photons escape from scintillator material, we observe a contribution on Compton continuum;
2) if only one escapes, there is a contribution on the peak corresponding to 0.511 MeV;
3) if no photon escapes, the share will be on the full energy peak.

Light Yield measurement is performed by full energy peak position determination using known energy gamma sources.

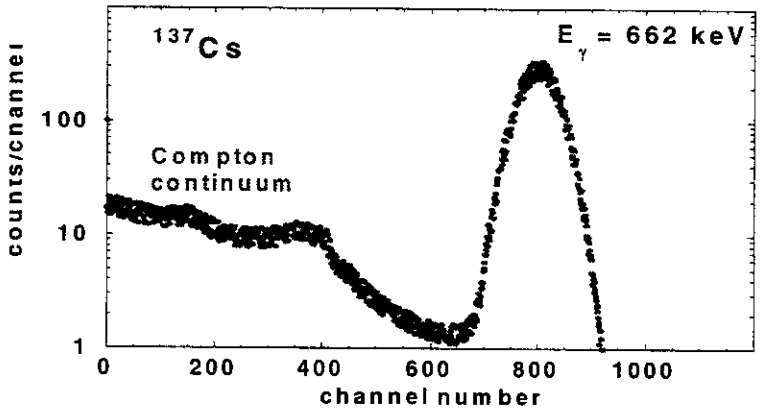

Fig. 3.3: Gamma spectrum of scintillating crystal (BGO) with ^{60}Co source.

^{60}Co, ^{22}Na and ^{137}Cs are commonly used radioactive sources. These are monochromatic sources, that emit known energy gamma rays: 0.511 MeV and 1.275 MeV (^{22}Na); 0.662 MeV (^{137}Cs); 1.173 MeV and 1.333 MeV (^{60}Co). LY value of scintillator materials is calculated from the ratio between photoelectrons number corresponding to the photoelectric peak and photons energy absorbed by material in this process (divided by phototube quantic efficiency, defined as the probability for a photon to reach the photocathode and to extract an electron) [16]:

$$LY = \frac{N_{fotoelettroni}}{E_\gamma \cdot Q_{eff}} \qquad (3.2)$$

Chapter 4 - Experimental measurements and results

Generally irradiation induces, in solid scintillators, colour centres formation able to absorb visible light, influencing energy resolution. Hence, scintillator radiation hardness represents a fundamental parameter; it is necessary to investigate this aspect when detector works in hostile environment. All glassy scintillators studied in this work, are characterised by doping with gadolinium and other rare earth ions, able to activate luminescence processes in the matrix [17, 18]. Gadolinium ion has an essential role in glassy system because it efficiently absorbs radiation energy and afterwards transfers this energy to glass matrix scintillating centres. Besides, energy migration process is observed between gadolinium ions before make over energy to activator ions. Hence, gadolinium amount in glass matrix influences considerably scintillator time decay: in fact, substituting gadolinium ions with optical inactive ions, distance Gd-Gd increases, so energy migration and decay kinetic decrease. It is not possible increase too much gadolinium quantity in glass matrix because it may induce trapping centres formation, causing an inefficient energy transfer towards the emission centres [19]. Gadolinium amount in glass matrix and stoichiometric ratio Gd/activator ion will determine an improvement or a worsening of scintillator performances.
The aim of this work is to study the dependence of silicate and phosphate glasses radiation hardness on the dopant (cerium or terbium) concentration and on glass matrix composition.

4.1 Samples and experimental set-up

In this work we studied two different kind of doped glass matrices: cerium-doped phosphate glasses (density around 4.5-5 $g \cdot cm^{-3}$), that could be used for low energy detection (up to 1 MeV) and terbium or cerium-doped silicate glasses (density around 3 $g \cdot cm^{-3}$), used for X-ray detection.

Silicate glasses

These samples are four oxides-based glasses produced (in controlled reducing atmosphere furnace) in the Stazione Sperimentale del Vetro (Murano, Italy) with different percentage of $Gd^{3+}$and Tb^{3+} or Ce^{3+} as activator ions. Denomination of the samples, their percentage composition and their length are shown in Table I. Percentage composition is reported as weight % of the starting materials (Gd_2O_3, Tb_2O_3, Ce_2O_3) in the primitive melt.

Phosphate glasses

These samples are three phosphates-based glasses produced in the Institute of Physics (Prague) with different percentage of $Gd^{3+}$and Ce^{3+}, as shown in Table II. In this case, the percentage composition denote the molar percentage of the starting materials in the melt ($NaPO_4$, $GdPO_4$ and $CePO_4$). These constituents were melted in a quartz ampoule around 1200°C and then poured into a graphite crucible. The production of these glasses is rather difficult since a large amount of Ce^{3+} causes devitrification and possible formation of Ce^{4+}, able to absorb Ce^{3+} scintillating light.

Table I

Sample denomination	Composition (wt%)	Lenght (mm)
VNL21	$10\%Tb_2O_3$, $22\%Gd_2O_3$	15.0
VNL22	$25\%Gd_2O_3$	15.0
VNL23	$3\%Tb_2O_3$, $24\%Gd_2O_3$	15.0
VNL6	$4.5\%Ce_2O_3$	20.0

Table II

Sample denomination	Composition (molar %)	Length (mm)
VNL3	25% $GdPO_4$, 1%$CePO_4$	22.0
VNL4	25% $GdPO_4$	28.0
VNL5	1%$CePO_4$	40.5

To evaluate quantitatively colour centres formation by irradiation, we used the radiation induced coefficient, μ. Moreover, to compare optical properties of samples having different lengths (L), we calculated the quantity ε, proportional to the absorbance, defined as:

$$\varepsilon\left[m^{-1}\right]=\frac{1}{L}\ln\left(\frac{100}{T\%}\right) \tag{4.1}$$

where T% stands for transmission before irradiation.
Samples were irradiated using a gamma source (^{60}Co, Calliope irradiation plant in ENEA, Casaccia, Italy) [20] in equilibrium charge particles condition and after dosimetric measurement for dose rate determination. No recovery components were observed in transmission spectra of samples after irradiation (until 7 days from the end of irradiation), then we could assume that the irradiation effect is independent on the dose rate. Hence, irradiation of phosphate glasses at lower doses (1-10 Gy) were performed in the dosimetric point corresponding to 0.46 Gy/h, while tests at higher doses (10-260 Gy) were performed in the dosimetric point corresponding to 4 Gy/h. After irradiation, every sample was thermally bleached by heating for 2-3 hours at temperature of 240°C for phosphates and 450°C for silicates.

4.2 Radiation damage measurements

Silicates glasses doped with terbium

In Fig. 4.1 transmission curves of samples VNL21, VNL22, VNL23 are shown.

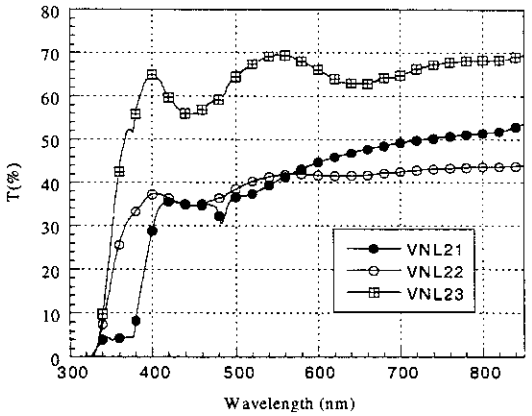

Fig. 4.1: Transmission curves of silicates glasses.

As can be seen, samples containing Gd only as well or a 3% $Tb^{3+}$are characterised by a band-edge around 330 nm, while sample containing the higher concentration of Tb^{3+} (10%) presents a little knee around 330-380 nm (corresponding to a transmission value around 5%) with a significant increase in transmission located around 380 nm. This evidence can be explained,

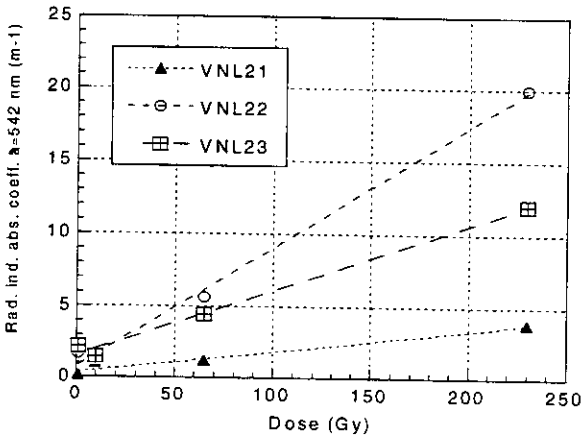

Fig. 4.4: Induced absorption coefficient, at λ emission, of silicate glasses.

We reported the coefficient μ [m^{-1}] after 230 Gy irradiation dose for all sample at λ emission of terbium (482 nm, 542 nm, 585 nm, 621 nm) in Table III.

Table III

Sample	μ at λ=482 nm	μ at λ=542 nm	μ at λ=585 nm	μ at λ=621 nm
VNL3	16.70±1.50	3.89±1.05	2.23±0.94	1.73±0.89
VNL4	38.60±1.50	19.90±1.10	11.65±1.03	8.71±1.02
VNL5	20.61±0.80	12.00±0.64	9.41±0.64	7.87±0.67

Phosphate glasses doped with cerium

In Fig. 4.5 the ε curves of VNL3, VNL4 and VNL5 samples are reported. It is evident that the sample containing only Gd^{3+} rare earth ion is characterised by a band-edge around 300 nm, while the other samples containing Ce^{3+} or both Ce^{3+}-Gd^{3+} ions are characterised by a slightly shifted band-edge (320 nm) towards visible region of the spectrum. Irradiation induces a decrease in transmission proportional to the dose and depending on glasses composition.

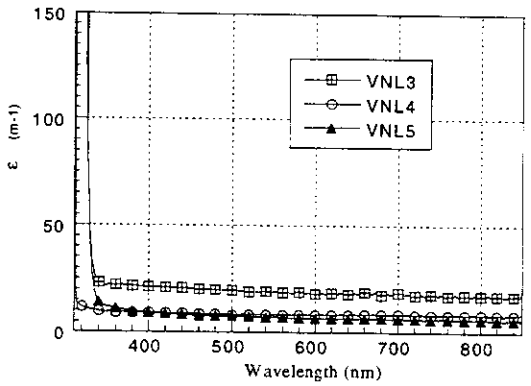

Fig. 4.5: ε curves of phosphate glasses.

Samples doped (or co-doped) with Ce^{3+}show a decrease in transmission more evident in UV region (320-380 nm) (Fig 4.6), while for the Gd^{3+} doped sample the decrease extends from 300 to 600 nm (Fig. 4.7) and it is more pronounced around 500 nm.

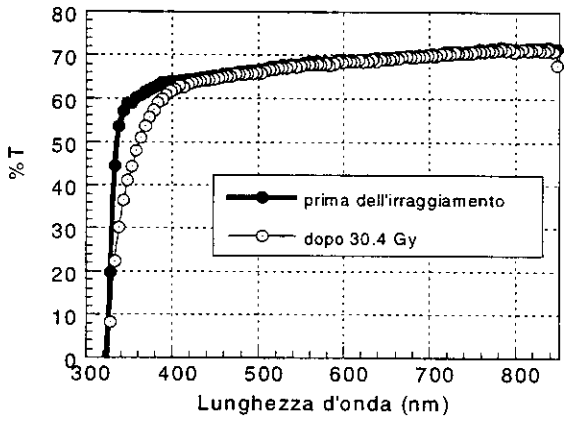

Fig. 4.6: Transmission curves before and after irradiation of silicates containing Gd and Ce.

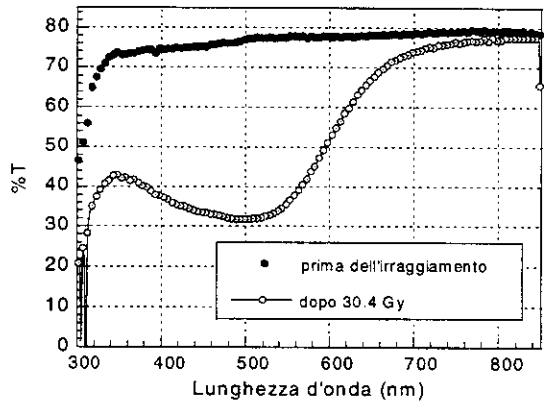

Fig. 4.7: Transmission curves before and after irradiation of silicate containing only Gd.

From the application point of view the wavelengths of interest are obviously the ones at which the scintillator emits (350 nm for Ce^{3+} and 309 nm for Gd^{3+}). For this reason in Fig. 4.8 the radiation induced coefficients of samples at the proper scintillating wavelength are reported: it is evident that Gd^{3+} doped sample is less resistant to radiation respect to sample containing Ce^{3+}, while the coefficient μ of other samples are practically identical.

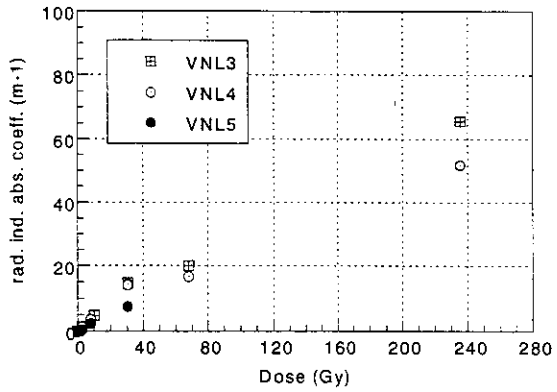

Fig. 4.8: Radiation induced absorption coefficient of phosphate glasses at emission λ.

The role of cerium in silicate and phosphate matrix

To get some more insight about the role of Ce^{3+} in silicate and phosphate matrix, we have compared the results obtained on the samples VNL5 and VNL6. When the ε curves are compared, it is evident that Ce^{3+} doped phosphate has a band-edge around 320 nm, while the Ce3+ doped silicate is characterised by a band-edge around 360 nm (Fig. 4.9). Such result can be explained by higher crystal field in silicate glasses, which shifts to lower energy the 4f-5d absorption transition of Ce^{3+} ion. As far as the shape of radiation induced coefficient of both samples, we can observe that it is approximately the same, with some shift towards the UV region in the phosphate sample. Comparing the radiation coefficient of both samples at the wavelengths of interest (350 nm for phosphates and 410 nm for silicates) one can conclude that the radiation hardness of considered phosphate and silicate samples is comparable.

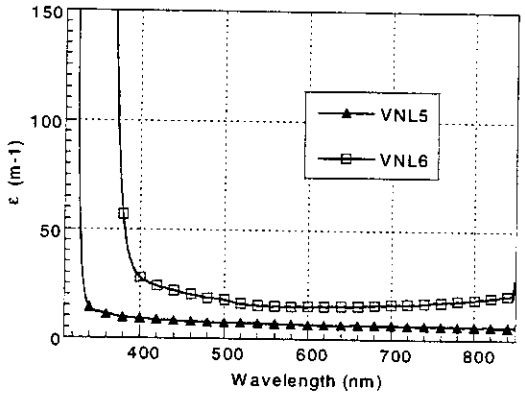

Fig. 4.9: ε curves of silicate and phosphate glasses cerium-doped.

4.3 Luminescence measurements

From the optical properties point of view, glasses matrices were characterised by absorption and emission spectra, and by kinetics studies in the luminescence decay; used experimental set-up are described below.

In collaboration with the Institute of Physics (Prague), emission spectra (at RT and under X-ray excitation) of Ce^{3+}-doped silicate glasses are obtained [23]. In Fig. 4.10 phosphates emission spectra are reported, with typical cerium emission band around 350 nm.

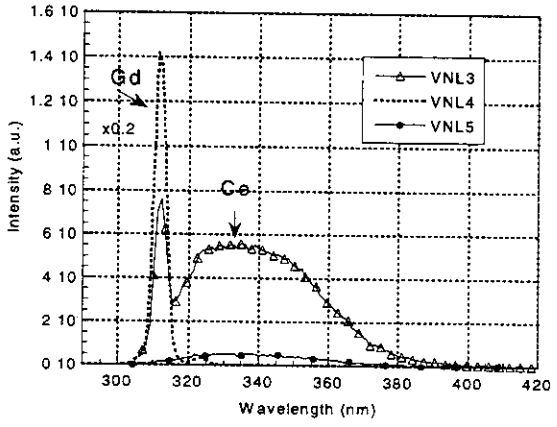

Fig. 4.10: Emission spectra of silicate glasses cerium-doped.

Cerium centres luminescence decay (obtained using a XeCl laser, 308 nm) is characterised by a fast component (about 20-30 nm) and by a non-exponential slow component, as shown in

Fig. 4.11. It is evident that, at higher temperature, the last one increases considerably. This behaviour can be explained considering that, at room temperature, energy can be transferred from cerium ions to gadolinium ones (back energy transfer). In the cerium decay, appearance of components (6.5 ms) longer than normal cerium emission ones (0.52 ms) represents the evidence of direct energy transfer $Gd^{3+} \rightarrow Ce^{3+}$. Similarly, in the case of Tb-doped phosphate glasses, VNL22 sample (containing gadolinium only as well) presents a time decay of about 2.1 ms, while for VNL21 sample (10% Tb) time decay is nearly 0.02 ms [21, 24]. Besides, comparing emission spectra shown in Fig 4.3, energy transfer $Gd^{3+} \rightarrow Tb^{3+}$ is evident [25].

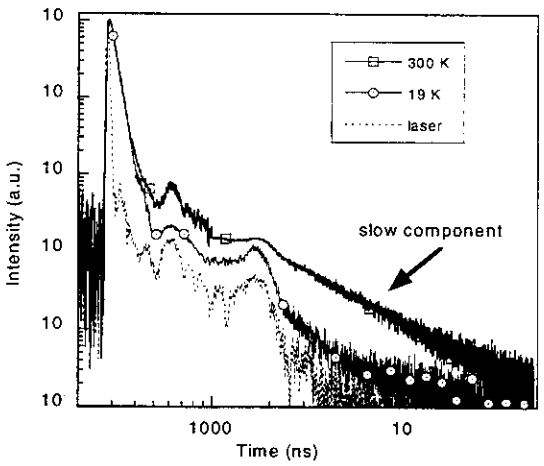

Fig. 4.11: Photoluminescence decay of phosphate glasses at different temperature and at λ=350 nm.

4.4 Light Yield measurements

To evaluate scintillator emitted light, all samples were measured by a Light Yield experimental set-up. The obtained LY value is practically equal to zero for all analysed glasses. For samples containing cerium, this result can be explained considering the low intensity of cerium emitted light; in fact, whether samples containing only cerium (VNL5, VNL6) or samples containing also a little gadolinium amount (VNL3), the luminescence efficiency is too low to produces detectable signal.

For Tb-doped silicate glasses, integration time used in experimental set-up is too short to permit the terbium emitted light integration because terbium emission time is around ms.

Conclusions

We can conclude that the optical properties of analysed glasses are strictly correlated with their composition: particularly, phosphate glasses containing cerium present a transmission decrease especially in UV region, while for Gd-doped glasses this decrease is extended between 300 nm and 600 nm with a peak around 500 nm. For silicate glasses, transmission decreases in UV region independently from doping. From the luminescence measurements point of view, we observed back energy transfer $Ce^{3+} \rightarrow Gd^{3+}$, that introduces slow components in activator decay. Further studies might consist in the optimisation of stoichyometric ratio Gd/activator ion in different glass matrices.

Acknowledgements

The authors are grateful to Angelo Pasquali, Francesco Zarbo and Dott. Armando Festinesi (ENEA-Casaccia Research Centres) for their collaboration in the realisation of this work. A special thank is devoted to Dott. G.Paolo Pazzi and Dott. Pasquale Fabeni from IROE-CNR and Dott. Martin Nikl from Academic Science of Prague, for their scientific support.

References

[1] WILLIAMS F., "Theoretical Basis for Solid State Luminescence", in *Luminescence of Inorganic Solids*, P. Goldberg (Ed.), Academic Press, 1996.

[2] KNALL G., *Radiation Detection and Measurements*, Canada, John Wiley & Sons, 1979.

[3] KITTEL C., *Introduzione alla fisica dello stato solido*, Ed. Boringhieri, 1971.

[4] SCHULMAN J.H., W.D. COMPTON, *Colour Centres in Solids (International Series of Monographs on Solid State Physics)* 2, Pergamon Press, 1962.

[5] PRIZBRAM K., *Irradiation Colour and Luminescence*, London, Pergamon Press, 1956.

[6] RINDONE G.E., "Luminescence in Glassy State", in *Luminescence of Inorganic Solids*, P. Goldberg (Ed.), Academic Press, 1996.

[7] BLASSE G., "Luminescence and Scintillation Mechanism in Inorganic Scintillator", *Proc. of the "Crystal 2000" International Workshop*, Chamonix (France), september 1992.

[8] PELLICCIONI M., *Fondamenti fisici della radioprotezione*, Bologna, Pitagora editrice, 1993.

[9] SEGRE' E., *Nuclei e particelle*, Bologna, Zanichelli, 1982.

[10] STERNHEIMER R.M., "Interaction of Radiation with Matter", in *Method of experimental physics:nuclear physics*, vol. 5A, New York, L.C.L. Yuan e C.S. Wu (Eds.), Academic Press, 1962.

[11] PRICE W.J., *Rivelazione della radiazione nucleare*, Roma, Bulzoni editore, 1972.

[12] LEO W.R., *Techniques for Nuclear and Particles Physics Experiments*, Springer Verlag, 1991.

[13] ATTIX F.H., W.C. ROESCH, "Basic Concepts of Dosimetry", in *Radiation dosimetry*, 2, F.H. Attix e W.C. Roesch (Eds.), New York, Academic Press, 1966.

[14] BACCARO S., L.M. BARONE, B. BORGIA, F. CASTELLI, F. CAVALLARI, I. DAFINEI, F. DE NOTARISTEFANI, M. DIEMOZ, A. FESTINESI, E. LEONARDI, E. LONGO, M. MONTECCHI, G. ORGANTINI, "Ordinary and Extraordinary Complex Refractive Index of the Lead Tungstate ($PbWO_4$) Crystal", *NIM A 385*, 1997.

[15] COZZI R., P. PROTTI, T. RAUTO, *Analisi chimica e moderni metodi sperimentali*, Zanichelli, Bologna, 1993.

[16] BACCARO S., L.M. BARONE, B. BORGIA, F. CASTELLI, F. CAVALLARI, F. DE NOTARISTEFANI, M. DIEMOZ, R. FACCINI, A. FESTINESI, E. LEONARDI, E. LONGO, M. MONTECCHI, G. ORGANTINI, L.

PACCIANI, S. PIRRO, "Precise Determination of the Light Yield of Scintillating Crystals", *NIM A 385*, 1997.

[17] NELSON W.F., S.W. BARBER, R.J. BIERINGER, F.T. KING, "Optical Properties of the Rare Earths when Doped into Pure Fused Silica", *Proc. Int. Conf. on Physics of Non Crystalline Solids*, Amsterdam, North Holland Publishing Company, 1965.

[18] DUJARDIN C., C. PEDRINI, M. MOYSAN, J.Y. CARREE, G. MAZE', J. JIANG, G. ZHANG, M. POULAIN, "Scintillation Properties of Heavy Cerium-Doped Glasses", *Proc. Int. Conf. of Inorganic Scintillators and their Application, SCINT97*, CAS Shangai Branch Press, 1997.

[19] BACCARO S., R. DALL'IGNA, P. FABENI, M. MARTINI, J.M. MARES, F. MEINARDI, E. MIHOCOVA, M. NIKL, K. NITSCH, G.P. PAZZI, P. POLATO, A. VEDDA, G. ZANELLA, R. ZANNONI, "High Light Yield Ce^{3+} (Tb^{3+})-doped Phosphate and Oxide Scintillation Glasses", will be published on *Proc. of SCINT99*, Moscow, 16-20 August 1999.

[20] BACCARO S, B. BORGIA, A. FESTINESI, "Gamma and Neutron Irradiation Facilities at ENEA-Casaccia Centre (Rome)", *CERN-CMS Note*-1995/192.

[21] BACCARO S., A. CECILIA, R. DALL'IGNA, P. FABENI, M. MARTINI, J.M. MARES, E. MIHOCOVA, M. MONTECCHI, M. NIKL, P. POLATO, A. VEDDA, G. ZANELLA, R. ZANNONI, "Radiation Damage of Ce^{3+} (Tb^{3+})-doped Phosphate and Oxide Scintillating Glasses", will be published on *Proc. of SCINT99*, Moscow, 16-20 August 1999.

[22] BETTINELLI M., G. INGLETTO, P. POLATO, G. POZZA, G. ZANELLA, R. ZANNONI, *Phys. Chem. Glasses*, 37 (1), 4, 1996.

[23] BACCARO S., A. CECILIA, R. DALL'IGNA, P. FABENI, M. MARTINI, J.M. MARES,, F. MEINARDI, M. NIKL, K. NITSCH, G.P. PAZZI, P. POLATO, A. VEDDA, G. ZANELLA, R. ZANNONI, "Ce^{3+} or Tb^{3+}-doped Phosphate and Scintillating Glasses", will be published in *Journal of Luminescence*.

[24] B ETTINELLI M., P. POLATO, G. ZANELLA, R. ZANNONI, "Scintillating Glasses for X-ray and Neutron Detection", *Fundamentals of Glass Science & Technology 3rd ESG Conf.*, C1-571, 1995.

[25] MARES J.A., M. NIKL, C. PEDRINI, D. BOUTTET, C. DUJARDIN, B. MOINE, J.W.M. VERWEIJ, J. KVAPIL, *Radiation Effects and Defects in Solids*, 1995.